Applied Surface Science 297 (2014) 33–39

Contents lists available at ScienceDirect

Applied Surface Science

journal homepage: www.elsevier.com/locate/apsusc

Fabrication of a superhydrophobic surface from porous polymer using phase separation

Jianfeng Liu, Xinyan Xiao*, Yinlong Shi, Caixia Wan

School of Chemistry and Chemical Engineering, South China University of Technology, Guangzhou 510640, PR China

ARTICLE INFO

Article history:
Received 28 November 2013
Received in revised form 9 January 2014
Accepted 10 January 2014
Available online 20 January 2014

Keywords:
Superhydrophobic
Porous polymer
Porogen
Phase separation
Water contact angle

ABSTRACT

The present work reports a simple method to fabricate superhydrophobic porous polymeric surfaces by a phase separation process. The method involves the in situ polymerization of butyl methacrylate (BMA) and ethylene dimethacrylate (EDMA) in the presence of co-porogens of 1,4-butanediol (BDO) and *N*-methyl-2-pyrrolidone (NMP) to afford superhydrophobic surfaces with the micro/nano roughness structure. The influences of the polymerization mixture on the morphology and hydrophobicity were investigated by adjusting the composition of the co-porogens and the mass ratio of monomers to co-porogens, respectively. And a precise description of the underlying mechanism of the microstructure formation was presented. The as-prepared surface shows a superhydrophobicity with water contact angle (WCA) of 159.5° and low sliding angle (SA) of 3.1°. Moreover, the superhydrophobic surface shows good chemical stability with better resistance to acid, alkali or salt aqueous solutions and excellent thermal stability. The method is simple and low-cost and can be used for the preparation of the self-cleaning superhydrophobic surfaces.

1. Introduction

Superhydrophobic surfaces with water contact angle (WCA) larger than 150° and sliding angle (SA) lower than 10° have attracted considerable interest during the last years [1–5]. Their possible industrial and practical applications range from self-cleaning coatings, oil–water separation, and micro-fluidics to water-proof textiles [6–8]. In nature, many plants and animals exhibit superhydrophobic property, such as lotus leaves, rice leaves, red rose petals, gecko feet and desert beetle, and so on. The investigation of lotus leaves demonstrated that the combination of multi-scaled rough structure and the low surface energy compound is essential for superhydrophobicity [9]. In order to mimic the superhydrophobic effect, many approaches, such as sol–gel method [10], template method [11], solution immersion process [12,13], electrospinning [14], phase separation [15–19], polymer/nanoparticle composite [20] and laser method [21], have been developed. Among all these methods phase separation is a relatively facile, efficient, and low cost method to attain superhydrophobic surface. Aruna et al. [22] prepared polystyrene (PS) based superhydrophobic films by non-solvent induced phase separation method using tetrahydrofuran (THF) as the solvent and different alcohols as non-solvents. And the prepared coatings exhibited a maximum WCA of 159°. Pi et al. [23] prepared a polylactic acid (PLA) superhydrophobic film, in which a microphase separation happened during the film drying and the polyethylene oxide (PEO) formed microdomains for the dissimilarity of PLA and PEO. Finally, a porous and rough PLA film formed. Wei et al. [24] synthesized copolymers of styrene and 2,2,3,4,4,4-hexafluorobutyl methacrylate by bulk polymerization firstly. The copolymer was dissolved in THF, and then added ethanol into the solution thereafter, to induce phase separation. The WCA and SA were measured as 154.3°and 5.8°, respectively. The microstructures of the polymer films were controlled by the degree of phase separation. However, some limits are associated with these methods, such as specific humidity, suitable solvent and non-solvent, or low surface energy compound. The stability of the surface hydrophobicity is also a great problem. In this study, a facile phase separation process to fabricate superhydrophobic polymeric surfaces is reported. The process involves in situ polymerization of monomers in the presence of co-porogens. The co-porogens in the polymerization mixture lead to phase separation when the growing cross-linked polymer chains achieve a critical length. In order to minimize the surface energy, the precipitates of the polymer chains will reunite into conglomerations,

Abbreviations: BMA, butyl methacrylate; EDMA, ethylene dimethacrylate; BDO, 1,4-butanediol; NMP, *N*-methyl-2-pyrrolidone; AIBN, 2,2′-azobisisobutyronitrille; WCA, water contact angle; SEM, scanning electron microscope; AFM, atomic force microscopy.

* Corresponding author. Tel.: +86 20 87112074.
E-mail address: cexyxiao@scut.edu.cn (X. Xiao).

0169-4332/$ – see front matter © 2014 Elsevier B.V. All rights reserved.
http://dx.doi.org/10.1016/j.apsusc.2014.01.053

and these small polymer conglomerations constitute the porous structure of the polymeric surface. The porous polymeric surface was formed directly on the substrate via in situ polymerization of monomers, and no further modification with low-surface-energy materials was needed in the following process. Thus it is reasonable to expect this method has a potential application in the preparation of superhydrophobic surface.

2. Experimental

2.1. Materials

Butyl methacrylate (BMA, chemical pure) was purchased from Shang Hai Linfeng Chemical Co. Ltd. Ethylene dimethacrylate (EDMA, chemical pure) was provided by Aladdin industrial Co. Ltd. 1,4-butanediol (BDO, analytical reagent), 2,2′-azobisisobutyronitrille (AIBN, analytical reagent) and *N*-methyl-2-pyrrolidone (NMP, analytical reagent), were obtained from Tian Jing Kermel Chemical Co. Ltd. The other reagents used were as follows: methanol (analytical reagent), 3-(trimethoxysilyl) propyl methacrylate (KH-570, commercial grade). All the materials were used without further purification.

2.2. Preparation of polymeric surfaces

The surfaces were prepared by an in situ polymerization on glass substrates. The polymerization mixture consisting of BMA, EDMA, BDO, NMP and AIBN (2 wt% with respect to the mass of BMA and EDMA) was ultrasonically dispersed for 15 min in a beaker. Then a 0.25 mL of the mixture was injected into a mold assembled from a glass substrate (25.4 mm × 76.2 mm × 1.1 mm) pretreated by (0.2 mol L^{-1}) HCl solution, (1 mol L^{-1}) NaOH solution and KH-570 [25] and a Teflon board (115 mm × 50 mm × 3 mm), and the glass substrate was sealed around by using Teflon strips (as shown in Fig. 1). After thermally initiated polymerizations for 20 h at 75 °C, the glass substrate and Teflon board were carefully opened by a blade. The polymeric layer usually adheres to the glass substrate. Then the polymeric layer was submersed in methanol ultrasonically for at least 20 min at room temperature to remove the porogens and the residual monomers. Finally, the porous polymeric surface with an average thickness of 95 μm could be obtained by drying at room temperature.

2.3. Characterizations

WCA of the surfaces was measured with an OCA20 contact angle goniometer (Dataphysics Co. Germany) by sessile drop method at 25 °C with 6 μL of water droplet. The obtained WCA is the average of five measurements on different areas of the measured surface. The sliding angle (SA) is defined as the slope angle where the water droplet begins to roll off the gradually inclined surface. And SA of the polymer surface was measured at 25 °C with a 10 μL of water droplet.

The microstructure of the surfaces was observed by scanning electron microscope (SEM, S3700 Hitachi) at an accelerating voltage of 10 kV. Prior to SEM characterization, the sample was coated with a thin layer of gold.

The morphology of the surfaces was examined using atomic force microscopy (AFM, CSPM2003) with tapping mode. The roughness parameters of the surfaces could be calculated by Imager 4.60 software from the data of AFM images.

The monomer conversion was determined from the equation (1):

$$\eta = \frac{m_1 - m_2 - m_3}{m_0} \times 100\% \quad (1)$$

where η is the monomer conversion, m_0 is the monomer weight of BMA and EDMA, m_1 is the weight of the polymeric layer and glass substrate after methanol washing at least 20 min and drying at 75 °C in the oven until a constant weight is obtained, m_2 and m_3 are the weights of the glass substrate and the initiator, respectively.

3. Results and discussion

3.1. Effect of the co-porogens

Porogen is commonly used in the preparation of the porous polymers, which has a prominent impact on the microstructure of the porous polymers [26]. Usually, two or more different polar porogens (solvents) are chosen as co-porogens, the aim is to assist in the preparation of a bimodal pore structure that will afford to improve the porosity of the polymer material. Various polymer surfaces with different average pore size and polymeric conglomeration size can be designed and prepared by adjusting the polarity of the co-porogens. Thus, porous polymer surfaces are obtained by adjusting the mass ratio of BDO to NMP ranging from 30:70 to 60:40, and an increase of the polarity of the co-porogens is caused by increasing the content of BDO.

Keeping the ratio of monomers to co-porogens at 45:55 and BMA to EDMA at 50:50, the SEM images of the prepared surfaces are shown in Fig. 2, in which the ratio of BDO to NMP is 30:70 (Fig. 2(a and b)), 40:60 (Fig. 2(c and d)), and 50:50 (Fig. 2(e and f)), respectively. It can be seen from Fig. 2 that the average pores size and polymeric conglomerations size of the surfaces become large gradually with the ratio of BDO to NMP increasing. Usually, the polymer has the relatively high solubility in a low polarity solvent, and phase separation will occur late in the polymerization process. When the phase separation began, the polymerization mixture becomes highly viscous, and the diffusion of remaining monomers and short-chain polymers is difficult. The phase separation occurs at the local scope of the polymerization mixture. Finally, a fine network with small pores and polymeric conglomerations is formed, as can be seen from Fig. 2(a and b). While the polymer has the relatively low solubility in a high polarity solvent, and phase separation will occur at the early stage of the polymerization process. Monomers can still diffuse over longer distances to the primary regions of polymeric phase, and the monomers prefer to polymerize at the interface of the polymeric phase in order to reduce the surface free energy. As a result, the large size of the conglomerations and pores will be formed, as can be seen from Fig. 2(e and f). So, an increase of the polarity of co-porogens can result in an increase in the average size of pores and polymeric conglomerations.

The effect of BDO to NMP ratio on the hydrophobicity of the porous polymeric surfaces was investigated, and the results are shown in Fig. 3. As can be seen from Fig. 3, the WCA of the surfaces increases firstly and then decreases with the ratio increasing. When the ratio is 40:60, the surface shows highest WCA of 159.5°. With the ratio of BDO to NMP continuing to increase, the hydrophobicity of the surfaces begins to decline. It is explained as that the further increase of the average size of pores and conglomerations caused by increasing the dosage of BDO is not beneficial to the hydrophobicity of the surfaces.

3.2. Effect of the monomers to co-porogens ratio

The mass ratio of monomers to co-porogens is also an important factor that affecting the microstructure of the polymeric surfaces. Previous research has shown that the porogen content has an effect on the density of polymeric materials [27]. Keeping the mass ratio of BMA to EDMA at 50:50 and BDO to NMP at 40:60, the SEM images of the polymeric surfaces are shown in

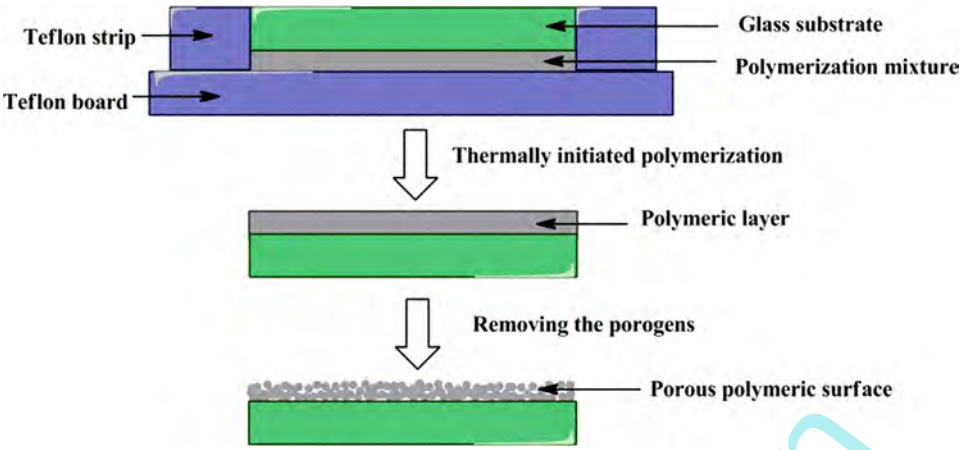

Fig. 1. Schematic representation of the fabrication of a porous polymeric surface on the glass substrate.

Fig. 4, in which the ratio of monomers to co-porogens is 20:80 (Fig. 4(a)), and 55:45 (Fig. 4(b)), respectively. It can be seen that Fig. 4(a) shows a much finer structure and smaller conglomeration size than that of Fig. 4(b). This phenomenon could be explained as that the phase separation behavior in a mixture with a low monomer concentration will occur later in the polymerization process than that with a high monomer concentration. As a result, the smaller pore size and conglomeration size formed. Fig. 4(a) has a lower density polymeric surface structure than that of Fig. 4(b), for the porogen does not participate in the polymerization reaction during the polymerization process, in which it is just surrounded by the mixture of polymerized monomers and removed by methanol washing finally. Thus the more the dosage of co-porogens is added, the lower density structure the polymeric surface has.

The effect of the ratio of monomers to co-porogens on the hydrophobicity of the porous polymeric surfaces was investigated, and the results are shown in Fig. 5. It can be seen that the WCA of the surfaces increases from 147.0° to159.5° firstly and then decreases from 159.5° to 144.7° with the content of co-porogens increasing.

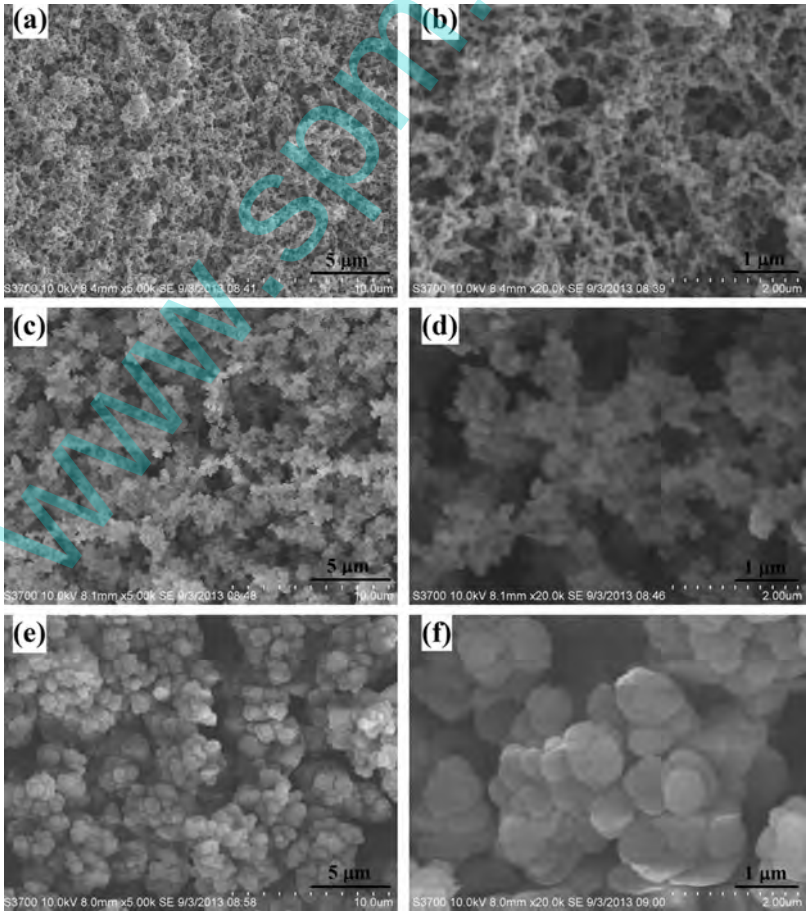

Fig. 2. SEM images of the surfaces with different mass ratio of BDO to NMP: (a and b) 30:70, (c and d) 40:60 and (e and f) 50:50; magnification: (a, c and e) 5.00K× and (b, d and f) 20.0K×.

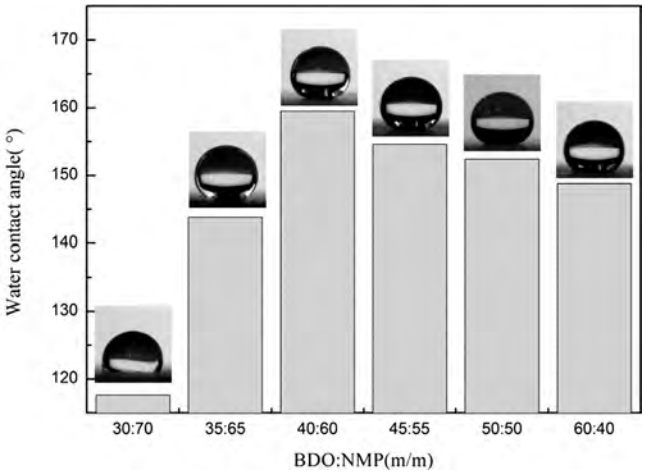

Fig. 3. The effect of the mass ratio of BDO to NMP on the hydrophobicity of the porous polymeric surfaces.

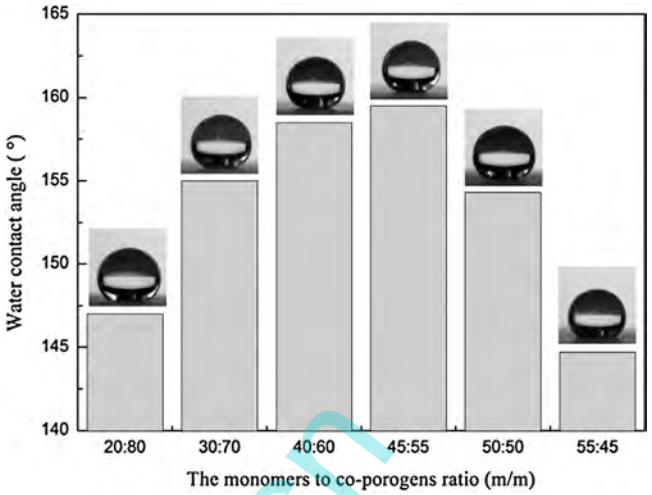

Fig. 5. The effect of the ratio of monomers to co-porogens on the hydrophobicity of the porous polymeric surfaces.

When the ratio of monomers to co-porogens is 45:55, the surface shows the highest WCA of 159.5°. This is probably due to that the pore size and conglomeration size of the surface are small when the ratio of monomers to co-porogens is less than 45:55 (as shown in Fig. 4(a)), so the roughness of the polymeric surface is not enough for reaching the superhydrophobic effect. The WCA of the surfaces decreases gradually when the ratio is more than 45:55. This is because the degree of phase separation of the polymer is weak when a small dosage of co-porogens is used and the formed structure of the polymer surface has fewer pores (as shown in Fig. 4(b)). This situation leads to the reduction of the proportion of air–liquid contact area in the composite surface, while this kind of surface structure is not suitable for superhydrophobic surface.

3.3. The monomer conversion

Keeping the reaction temperature at 75 °C, the mass ratio of BMA to EDMA, BDO to NMP and monomers to co-porogens at 50:50, 40:60, and 45:55, respectively, the effect of polymerization time on the monomer conversion is shown in Fig. 6. It can be seen from Fig. 6 that, the monomer conversion is 80.5% when the reaction time is 4 h, meaning that the reaction proceeds successfully under the given conditions; the monomer conversion reaches 95.0% when the reaction time is 12 h; and no significant change of the monomer conversion is observed with increasing of the reaction time. Although the monomer conversion is close to quantitative after 12 h, the hydrophobicity of the polymeric surface is still affected if the reaction system is kept longer at 75 °C of the polymerization temperature.

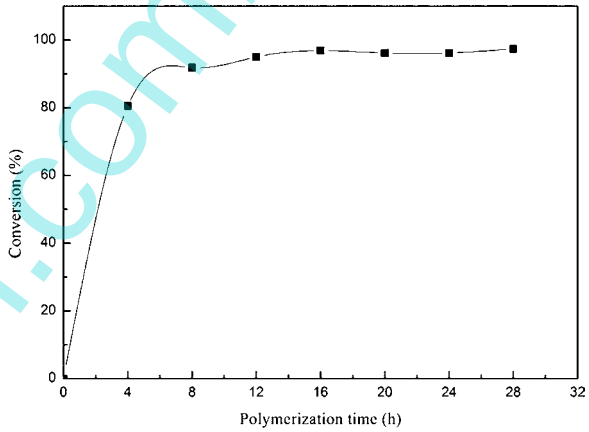

Fig. 6. The effect of polymerization time on the monomer conversion.

3.4. Micro-morphology of the polymeric surface

It is known that the roughness of the surface is an important factor to the hydrophobicity of a polymer surface. A smooth surface can be obtained when BMA and EDMA polymerize without any porogen, and only WCA of 85.8° of the resulting surface can be obtained (as shown in Fig. 7(a)). By the introducing of an optimal content of co-porogens into the polymerization mixture, the resulting superhydrophobic surface shows a highly porous structure with polymeric conglomerations randomly stacked over the surface (as shown in Fig. 7(c)). Fig. 7(b) and (d) show the AFM

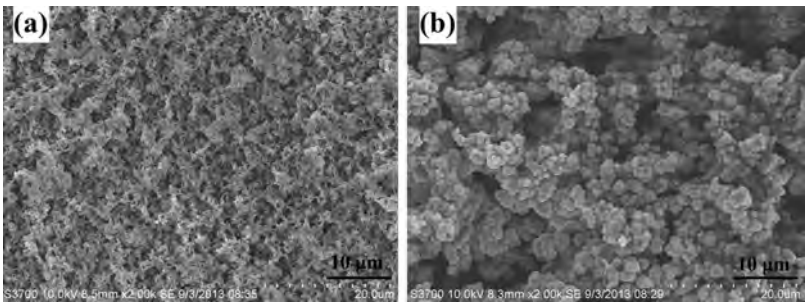

Fig. 4. SEM images of the surfaces with different mass ratio of the monomers to co-porogens: (a) 20:80, (b) 55:45; magnification: (a and b) 2.00K×.

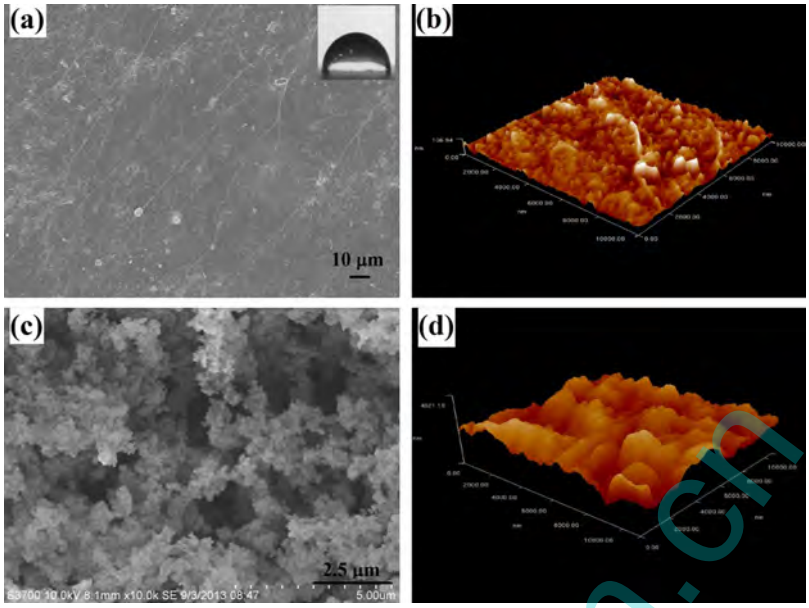

Fig. 7. SEM and AFM images of the polymeric surfaces prepared by polymerizing (a and b) without porogen, (c and d) with porogen. Inset is a water drop on the polymeric surface (a); SEM magnification: (a) 0.5K× and (c) 10.0K×.

Table 1
Roughness parameters for the polymeric surfaces.

Samples	S_a (roughness average) (nm)	S_q (root mean square) (nm)	S_{dr} (surface area ratio)	S_d (average diameter of peaks) (nm)	S_h (average height of peaks) (nm)	S_y (peak–peak) (nm)
The smooth surface	9	12	5	57	62	107
The superhydrophobic surface	413	507	142	438	2961	2780

images corresponding with Fig. 7(a) and (c), respectively. The result of preliminary quantitative analysis was obtained using Image 4.60 software, and it was shown in Table 1. It can be seen from Table 1 that the S_a (roughness average) and S_q (root mean square) of the smooth surface (Fig. 7(b)) is only 9 nm and 12 nm, respectively, so the surface is smooth and featureless which is correspond with the SEM analysis result (Fig. 7(a)). For the superhydrophobic surface (Fig. 7(d)), the S_d (average diameter of peaks), S_h (average height of peaks) and S_y (peak–peak) are 438 nm, 2961 nm and 2780 nm, respectively. Accordingly, the superhydrophobic surface shows the micro and nano-scale binary structure, similar to that of the lotus leaf. Also, the S_{dr} (surface area ratio, which is the ratio of the interfacial and projected areas) is 142, indicating the surface has a high surface roughness.

Additionally, the sliding angle (SA) is another important criterion for superhydrophobic surfaces. As shown in Fig. 8(a–c), the SA of a 10 μL water droplet on the resultant superhydrophobic surface is found to be as low as 3.1°, indicating a water droplet can roll

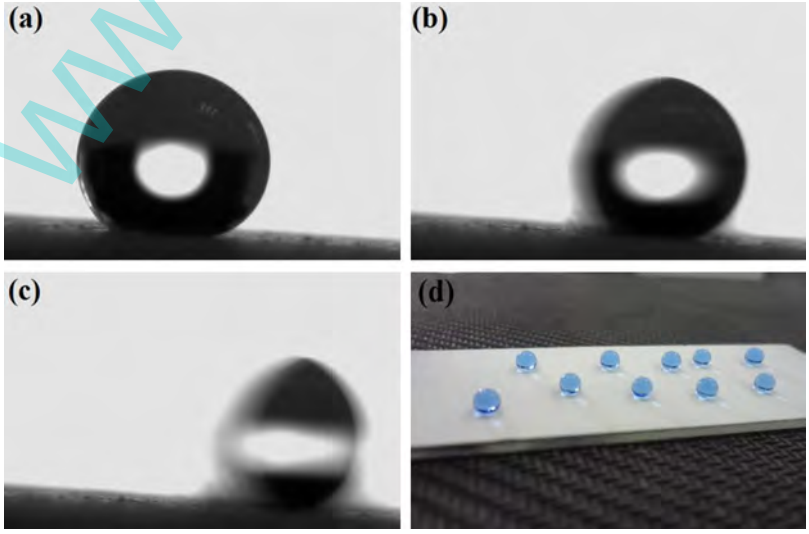

Fig. 8. Photographs of water droplets on the superhydrophobic porous polymeric surface. (a–c): sequential photographs of 10 μL water droplet rolling off the surface titled at 3.1°; (d): digital picture.

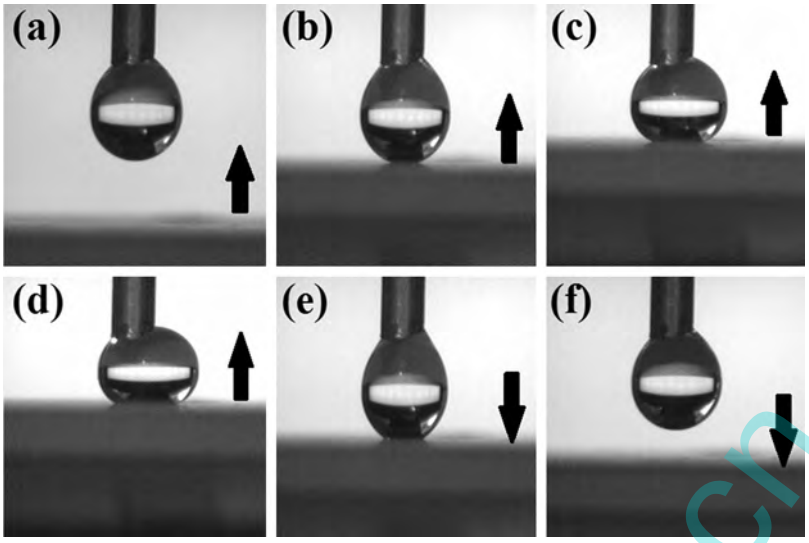

Fig. 9. The approach and departure process of an 8 μL water droplet from the superhydrophobic polymeric surface. The arrows represent the substrate's moving direction.

off the surface easily. So the superhydrophobic polymeric surface has great potential in self-cleaning application. Fig. 8(d) shows the digital picture of water droplets on the superhydrophobic polymeric surface.

The superhydrophobicity of the porous polymeric surface can be explained using Cassie–Baxter equation [28]:

$$\cos\theta^* = f_1 \cos\theta - f_2 \quad (2)$$

where f_1 and f_2 are fractions of the solid and air in the composite surface, respectively ($f_1 + f_2 = 1$).

Since the WCA values of the smooth polymer surface ($\theta = 85.8^\circ$) and rough superhydrophobic surface ($\theta^* = 159.5^\circ$) are given, f_2 is calculated to be 0.94. This means that air occupies about 94% of the contact areas when the water droplets contact with the binary roughness structured polymeric surface. Water droplets will keep spherical as much as possible under the action of surface tension, which makes the surface has a relatively high WCA and low SA.

3.5. The non-wetting property of the superhydrophobic polymeric surface

The non-wetting property of the superhydrophobic polymeric surface is analyzed using a method proposed by Gao and McCarthy [29]. Fig. 9 shows the approach, contact, deformation and departure processes of an 8 μL water droplet suspending on a syringe with respect to the porous superhydrophobic surface. It can be seen that the water droplet is difficult to be pulled down by the surface in all cases, with no visual water residue left. Moreover, the water droplet keeps almost sphere no matter whether it contacts with the surface slightly or severely, indicating that the adhesion force between the water droplet and the as-prepared surface is much weaker than that between the water droplet and the syringe. The non-sticking phenomenon also suggests that the superhydrophobic surface is in the Cassie–Baxter state in which water droplets rest on a layer of air.

3.6. The stability of the superhydrophobic polymeric surface

The as-prepared polymeric surface shows superhydrophobicity not only for pure water but also for corrosive solutions under different pH value. Fig. 10 shows the water droplets on the superhydrophobic surface after the polymeric surface was immersed in HCl solution (pH = 1), NaOH solution (pH = 14) and NaCl solution (pH = 7) for 8 h at room temperature, respectively. As is shown in Fig. 10, the WCA values of the polymeric surface are all higher than 150°. This means the prepared porous polymeric surface has good chemical stability to acid, alkali or salt aqueous solutions, which is of great important to the application of the superhydrophobic surface under corrosive condition.

The effect of treatment temperature on the WCA of the superhydrophobic surface is also studied. The surface was heated at different temperatures (from 125 °C to 225 °C) for 2 h. And WCA values were measured at 25 °C after each heat treatment. The results are shown in Fig. 11. When the temperature of thermal treatment is lower than 190 °C, WCA of the superhydrophobic polymeric surface is still higher than 150°. However, when the temperature is higher than 190 °C, WCA of the sample surface decreases. The reason is that the high temperature probably leads the micro-morphology of the polymeric surface damaged. Thus the superhydrophobic surface displays good thermal stability up to 190 °C.

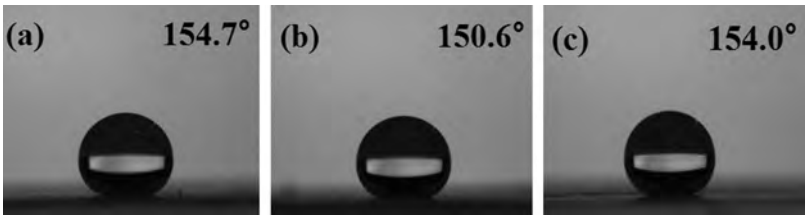

Fig. 10. The water droplet pictures on the superhydrophobic surface after the surface was immersed in (a) hydrochloric acid HCl solution (pH = 1), (b) sodium hydroxide NaOH solution (pH = 14) and (c) sodium chloride NaCl solution (pH = 7) for 8 h at room temperature, respectively.

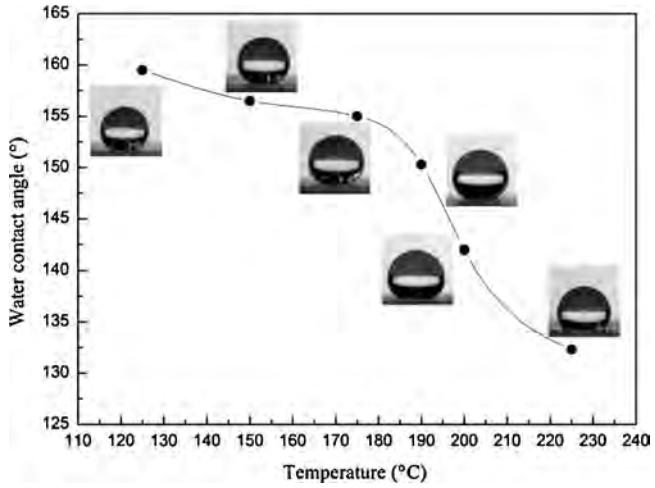

Fig. 11. The effect of treatment temperature on the WCA of the superhydrophobic polymeric surface.

4. Conclusions

Superhydrophobic porous polymeric surfaces were prepared by a simple phase separation method. The composition of the polymerization mixture has prominent influences on the morphology and hydrophobicity of the polymeric surfaces. SEM and AFM images of the superhydrophobic surface revealed its porous structure and micro/nano roughness structure. The polymeric surface shows a high water contact angle (WCA) of 159.5° and a low sliding angle (SA) of 3.1°, when the mass ratios of BMA to EDMA, BDO to NMP, and monomers to co-porogens are 50:50, 40:60 and 45:55, respectively. Meanwhile, the superhydrophobic surface shows good chemical and thermal stability.

Acknowledgment

This research was supported by the National Natural Science Foundation of China (21076092).

References

[1] X.Y. Lu, C.C. Zhang, Y.C. Han, Low-density polyethylene superhydrophobic surface by control of its crystallization behavior, Macromol. Rapid Commun. 25 (2004) 1606–1610.
[2] I. Yilgor, S. Bilgin, M. Isik, E. Yilgor, Facile preparation of superhydrophobic polymer surfaces, Polymer 53 (2012) 1180–1188.
[3] Z.G. Guo, F. Zhou, J.C. Hao, W.M. Liu, Stable biomimetic superhydrophobic engineering materials, J. Am. Chem. Soc. 127 (2005) 15670–15671.
[4] J.X.H. Wong, H.Z. Yu, Preparation of transparent superhydrophobic glass slides: demonstration of surface chemistry characteristics, J. Chem. Educ. 90 (2013) 1203–1206.
[5] G.M. Liu, L. Fu, A.V. Rode, V.S.J. Craig, Water droplet motion control on superhydrophobic surfaces: exploiting the Wenzel-to-Cassie transition, Langmuir 27 (2011) 2595–2600.
[6] M. Zhang, C.Y. Wang, S.L. Wang, Y.L. Shi, J. Li, Fabrication of coral-like superhydrophobic coating on filter paper for water–oil separation, Appl. Surf. Sci. 261 (2012) 764–769.
[7] Z. Mazrouei-Sebdani, A. Khoddami, Alkaline hydrolysis: a facile method to manufacture superhydrophobic polyester fabric by fluorocarbon coating, Prog. Org. Coat. 72 (2011) 638–646.
[8] X. Zhang, F. Shi, J. Niu, Y.G. Jiang, Z.Q. Wang, Superhydrophobic surfaces: from structural control to functional application, J. Mater. Chem. 18 (2008) 621–633.
[9] L. Jiang, Y. Zhao, J. Zhai, A lotus-leaf-like superhydrophobic surface: a porous microsphere/nanofiber composite film prepared by electrohydrodynamics, Angew. Chem. Int. Ed. 116 (2004) 4438–4441.
[10] J.B. Lin, H.L. Chen, T. Fei, C. Liu, J.L. Zhang, Highly transparent and thermally stable superhydrophobic coatings from the deposition of silica aerogels, Appl. Surf. Sci. 273 (2013) 776–786.
[11] T.C. Wang, L.J. Chang, S. Yang, Y. Jia, C.P. Wong, Hydrophobic properties of biomorphic carbon surfaces prepared by sintering lotus leaves, Ceram. Int. 39 (2013) 8165–8172.
[12] J. Li, Y.X. Yang, F. Zha, Z.Q. Lei, Facile fabrication of superhydrophobic ZnO surfaces from high to low water adhesion, Mater. Lett. 75 (2012) 71–73.
[13] Z.J. Cheng, M. Du, H. Lai, N.Q. Zhang, K.N. Sun, From petal effect to lotus effect: a facile solution immersion process for the fabrication of super-hydrophobic surfaces with controlled adhesion, Nanoscale 5 (2013) 2776–2783.
[14] S. Wang, Q.W. Liu, Y. Zhang, S.D. Wang, Y.X. Li, Q.B. Yang, Y. Song, Preparation of a multifunctional material with superhydrophobicity, superparamagnetism, mechanical stability and acids–bases resistance by electrospinning, Appl. Surf. Sci. 279 (2013) 150–158.
[15] P.A. Levkin, F. Svec, J.M.J. Fréchet, Porous polymer coatings: a versatile approach to superhydrophobic surfaces, Adv. Funct. Mater. 19 (2009) 1993–1998.
[16] Z.P. Fan, W.L. Liu, Z.J. Wei, J.S. Yao, X.L. Sun, M. Li, X.Q. Wang, Fabrication of two biomimetic superhydrophobic polymeric surfaces, Appl. Surf. Sci. 257 (2011) 4296–4301.
[17] N. Zhao, Q.D. Xie, L.H. Weng, S.Q. Wang, X.Y. Zhang, J. Xu, Superhydrophobic surface from vapor-induced phase separation of copolymer micellar solution, Macromolecules 38 (2005) 8996–8999.
[18] H. Nakanishi, T. Norisuye, Q. Tran-Cong-Miyata, Formation of hierarchically structured polymer films via multiple phase separation mediated by intermittent irradiation, J. Phys. Chem. Lett. 4 (2013) 3978–3982.
[19] Y.L. Peng, H.W. Fan, Y.J. Dong, Y.N. Song, H. Han, Effects of exposure time on variations in the structure and hydrophobicity of polyvinylidene fluoride membranes prepared via vapor-induced phase separation, Appl. Surf. Sci. 258 (2012) 7872–7881.
[20] F. Liu, S.L. Wang, M. Zhang, M.L. Ma, C.Y. Wang, J. Li, Improvement of mechanical robustness of the superhydrophobic wood surface by coating PVA/SiO_2 composite polymer, Appl. Surf. Sci. 280 (2013) 686–692.
[21] J.L. Yong, F. Chen, Q. Yang, D.S. Zhang, H. Bian, G.Q. Du, J.H. Si, X.W. Meng, X. Hou, Controllable adhesive superhydrophobic surfaces based on PDMS microwell arrays, Langmuir 29 (2013) 3274–3279.
[22] S.T. Aruna, P. Binsy, E. Richard, B.J. Basu, Properties of phase separation method synthesized superhydrophobic polystyrene films, Appl. Surf. Sci. 258 (2012) 3202–3207.
[23] P.H. Pi, W. Mu, G. Fei, Y.L. Deng, Superhydrophobic film fabricated by controlled microphase separation of PEO–PLA mixture and its transparence property, Appl. Surf. Sci. 273 (2013) 184–191.
[24] Z.J. Wei, W.L. Liu, D. Tian, C.L. Xiao, X.Q. Wang, Preparation of lotus-like superhydrophobic fluoropolymer films, Appl. Surf. Sci. 256 (2010) 3972–3976.
[25] C. Yu, M.H. Davey, F. Svec, J.M.J. Fréchet, Monolithic porous polymer for on-chip solid-phase extraction and preconcentration prepared by photoinitiated in situ polymerization within a microfluidic device, Anal. Chem. 73 (2001) 5088–5096.
[26] C. Viklund, E. Pontén, B. Glad, K. Irgum, P. Hörstedt, F. Svec, Molded macroporous poly (glycidyl methacrylate-*co*-trimethylolpropane trimethacrylate) materials with Fine controlled porous properties: preparation of monoliths using photoinitiated polymerization, Chem. Mater. 9 (1997) 463–471.
[27] S. Eeltink, J.M. Herrero-Martinez, G.P. Rozing, P.J. Schoenmakers, W.T. Kok, Tailoring the morphology of methacrylate ester-based monoliths for optimum efficiency in liquid chromatography, Anal. Chem. 77 (2005) 7342–7347.
[28] A.B.D. Cassie, S. Baxter, Wettability of porous surfaces, Faraday Soc. 40 (1944) 546–551.
[29] L.C. Gao, T.J. McCarthy, A perfectly hydrophobic surface ($\theta_A/\theta_R = 180°/180°$), J. Am. Chem. Soc. 128 (2006) 9052–9053.